Experimental and Theoretical Charge Density Study of Polymorphic Isonicotinamide−Oxalic Acid Molecular Complexes with Strong O···H···N Hydrogen Bonds

Marc Schmidtmann,[†] Louis J. Farrugia,[†] Derek S. Middlemiss,[†] Matthias J. Gutmann,[‡] Garry J. McIntyre,[§] and Chick C. Wilson*,[†]

WestCHEM, Department of Chemistry, University of Glasgow, Glasgow G12 8QQ, U.K., ISIS, Rutherford Appleton Laboratory, Chilton, Didcot, OX11 0QX, U.K., and Institut Laue-Langevin, BP 156, 38042 Grenoble Cedex 9, France

Received: July 17, 2009; Revised Manuscript Received: September 30, 2009

Two polymorphs of the 2:1 molecular complex of isonicotinamide and oxalic acid have been characterized by combined X-ray charge density and single-crystal neutron diffraction studies at 100 K. Both polymorphs show strong O−H···N intermolecular hydrogen bonding between the acid and the pyridine base. As is typical of short, strong hydrogen bonds (SSHBs), the covalent O−H bonds are considerably elongated to 1.161(3) and 1.235(5) Å, and the H···N interactions are correspondingly short at 1.398(3) and 1.313(6) Å in Forms I and II, respectively. The neutron diffraction data indicate no pronounced H dynamics in the SSHBs, and in the case of Form II the SSHB can be described as quasicentered. In addition to the experimental charge densities, theoretical charge densities have been determined from ab initio calculations within the full periodic environment of the crystalline state. The SSHBs are found to be covalent in nature according to the topological analysis of the experimental and theoretical charge densities and application of the source function. Aside from the SSHBs, moderate N−H···O and weak C−H···O interactions are also present in the molecular complexes, for which hydrogen bond energies are estimated from energy densities and independent ab initio calculations. Finally, an attempt is made to evaluate the intermolecular interactions governing the manifestation of polymorphism in this compound.

Introduction

The hydrogen bond (HB), denoted in the general form X−H···Y, is without doubt the most important intermolecular interaction. It is found in an abundance of materials, ranging from inorganic minerals to biologically active macromolecules. When present, HBs largely govern the structure of a wide range of materials, thereby contributing to the physical properties and (bio)chemical reactivity of the same. In this context, the short, strong hydrogen bond (SSHB) is of particular interest. It is found whenever the bonded atoms X, Y compete for the H atom, implying that the system is on the verge of exhibiting H transfer. Consequently, SSHBs in the solid state may be regarded as model systems for H transfer processes, effectively emulating the transition states of, for example, enzymatic reactions. SSHBs are energetically characterized by broad and flat potential energy profiles and small energy barriers for H transfer. Structurally, they are characterized by an elongated X−H covalent bond and a short H···Y hydrogen bonding interaction. In the extreme situation, the H occupies a centered position in the SSHB and is equally shared between the hydrogen bonded molecules, resulting in a centered SSHB (X···H···Y). In addition, competition for the H atom can also lead to equilibrium structures of the type X−H···Y ↔ X···H−Y. It has long been suggested that HBs, and in particular SSHBs, are at least partially covalent in nature. An overview of the early controversy surrounding the electrostatic and covalent HB model is given in "*The Hydrogen Bond*" by Pimentel and McClellan.[1] However, experimental evidence in favor of the covalent contribution to SSHBs in the solid state has lately emerged from analyses of the charge densities in strong homonuclear X−H···Y bonds.[2−8] Here, the topological analysis of the total electron density based on Bader's quantum theory of atoms in molecules (AIM)[9] has been employed to classify the HBs into the shared (mainly covalent) and closed shell (mainly electrostatic) types by evaluation of the properties of the H···Y bond critical point (BCP). The number of SSHBs which have been confirmed as covalent from experimental charge densities is, however, rather limited; this is due not only to the lack of compounds exhibiting covalent SSHBs but also to the lack of accurate H positional and displacement parameters, which, for strongly hydrogen bonded systems, can be derived only from single-crystal neutron diffraction experiments.

Here we present the results obtained from a combined charge density (experimental and theoretical) and single-crystal neutron diffraction study of the strongly hydrogen bonded 2:1 molecular complexes of isonicotinamide with oxalic acid $[C_5H_4NC(O)NH_2]_2\cdot(COOH)_2$ **1**. As reported earlier,[10,11] **1** crystallizes in two polymorphs, namely, Form I **1-I** and Form II **1-II** (Scheme 1). Upon substitution of the acidic hydrogen atoms with deuterium, two further deuterated polymorphs of $[C_5H_4NC(O)ND_2]_2\cdot(COOD)_2$ are obtained, neither of which are isostructural to the hydrogenous (^{1}H) forms.[12] The hydrogenous polymorphs exhibit intermolecular O−H···N SSHBs between both carboxylic acid groups and two molecules of isonicotinamide. In addition, moderate

* Corresponding author. E-mail: c.c.wilson@chem.gla.ac.uk. Tel.: +44 (0)141 330 8522. Fax: +44 (0)141 330 8775.
[†] University of Glasgow.
[‡] Rutherford Appleton Laboratory.
[§] Institut Laue-Langevin.

10.1021/jp9067813 CCC: $40.75
Published on Web 11/18/2009

SCHEME 1: Two Polymorphs of 1 Showing Their Hydrogen Bonding

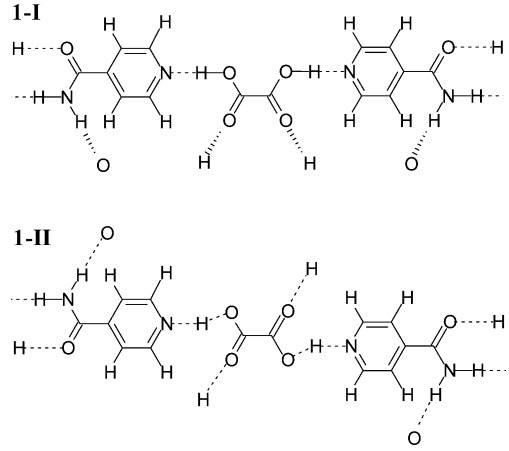

N−H···O and weak C−H···O HBs are present in **1**, offering the opportunity to study intermolecular hydrogen bonding spanning the whole energy spectrum from the very strong to the very weak in a polymorphic material. One aim of this work is to provide an accurate description of the electronic properties of the O−H···N SSHBs. A second aim is to attempt to evaluate the interaction energies governing the formation of the polymorphs, not only in regard to the SSHBs but also with respect to the weaker hydrogen bonding interactions.

Experimental Methods

Cocrystallization. 1-I and **1-II** were crystallized from stoichiometric ratios of isonicotinamide and oxalic acid dihydrate in water by slow isothermal evaporation. Both forms cocrystallize from the same batch but can be distinguished easily by their morphology. **1-I** crystallizes in the form of blocks (space group $C2/c$) and **1-II** in the form of needles or sticks (space group $P\bar{1}$). Also, **1-II** tends to crystallize prior to **1-I** but stops growing and disappears over a time scale of weeks when kept in solution subsequent to the formation of the first crystals of **1-I**, indicating that **1-I** is the thermodynamically more stable polymorph. When isolated from solution, however, **1-II** is stable and does not undergo a phase transition. Both polymorphs are stable in the temperature range from 30 K up to their respective melting points at approximately 500 K.

Neutron Diffraction. 1-I readily yields large single crystals suitable for neutron diffraction. The neutron data for this polymorph[11] were collected at 100 K on the time-of-flight (TOF) single-crystal Laue diffractometer (SXD)[13] at the ISIS neutron spallation source at the Rutherford Appleton Laboratory (RAL), U.K. A block-shaped sample with the approximate dimensions $3 \times 2 \times 2$ mm was used for the data collection. The data were processed with the program SXD2001,[13] a dedicated software package specifically developed for use with the SXD instrument. The resulting TOF multiwavelength data set consisted of 8486 observed ($F_{obs} > 4\sigma(F_{obs})$) reflections, and the structure was refined with the program SHELXL[14] to $R_1 = 0.0658$ for all reflections.

Growing neutron-sized crystals of **1-II** required the seeding of a saturated solution of isonicotinamide and oxalic acid with a small, needle-shaped specimen of **1-II**. The crystallization experiments yielded a multidomain crystal, several centimeters in length, from which a small block-shaped fragment ($0.8 \times 0.6 \times 0.4$ mm) was found suitable for data collection. The neutron data were measured at 100 K on the Very Intense Vertical Axis Laue Diffractometer (VIVALDI)[15] at the Institut Laue-Langevin (ILL) reactor source in Grenoble, France. The orientation matrices of the crystals were determined with the program LAUEGEN.[16] Since the Laue method at a continuous neutron source allows only relative linear cell dimensions to be determined, X-ray values were assumed in the neutron refinement of the cell parameters. 4633 reflections were integrated with ARGONNE_BOXES,[17] normalized to a common wavelength, scaled, and merged with LAUENORM[18] to yield a data set of 1915 unique reflections, of which 1365 are observed. Correction for absorption was deemed unnecessary in view of the small crystal size. While cooling slowly to 100 K, the crystal split into two domains, and the previously well-defined reflections at higher temperature (200 K) showed splitting into pairs arising out of the presence of a major and a minor component. However, the data set remains of sufficient quality to yield reasonable atomic parameters. The structure was refined with SHELXL against the merged data set to $R_1 = 0.0770$ and 0.1195 for the observed and all data, respectively. The crystallographic data and refinement details are summarized in Table 1.

X-ray Charge Density. The charge density experiments on both polymorphs of **1** were carried out on a Bruker AXS Apex II diffractometer at a temperature of 100 K, and the charge density refinements were carried out with the program XD2006,[19] which uses the standard Coppens−Hansen multipolar expansion[20] to model the charge density. The experimental data for **1-I** were integrated with SAINT[21] to sin $\theta/\lambda = 1.21$ Å^{-1} and scaled and corrected for absorption with SADABS.[22] The 62005 reflections thus obtained were subsequently merged with SORTAV[23] to generate a set of 9393 unique reflections. The initial model for the multipole refinement with XD2006 was taken from the result of the spherical atom refinement in SHELXL. The H parameters were taken from the model obtained from the neutron experiment at 100 K and were fixed during the refinement; the H atomic displacement parameters (ADPs) were additionally compared to the heavy atom ADPs obtained from the SHELXL refinement and scaled accordingly with the program UIJXN.[24] In the XD refinement, multipole expansions up to the octupolar level ($l = 3$) were included for the heavy elements (C, N, O) and up to the quadrupolar ($l = 2$) for H, but here only the bond directed quadrupoles were included, as suggested by Volkov et al.[25] No chemical constraints were employed in the refinement model, save that the contraction−expansion parameters (κ and κ') of chemically similar atoms were set equal, resulting in 9 κ sets for the 19 independent atoms (the H atom involved in the SSHB was assigned a unique κ set). The κ parameters for the spherical monopole terms (κ) were refined independently of those for the multipole terms (κ'), and the latter were held equal within each set. Statistical weights were applied. Although the data set is not complete in the very high resolution shells, the structure was refined against all $F_{obs} > 4\sigma(F_{obs})$. A total of 354 parameters were refined to $R_1 = 0.0159$ for the 7817 observed and unique data. The maximum and minimum residual densities are 0.155 and −0.146 e·Å^{-3} (rms = 0.029 e·Å^{-3}) calculated for all observed data on a 0.1 Å grid. The two strongest reflections (3 1 1 and 6 0 2) were omitted from the data set because their experimental intensities were significantly underestimated, most likely as a consequence of strong extinction, despite the use of an isotropic extinction correction (Becker−Coppens type 2[26]). The inclusion of the above reflections heavily biased the

TABLE 1: Crystallographic Data for 1

	1-I		**1-II**	
radiation	neutron[a]	X-ray	neutron[b]	X-ray
wavelength (Å)	0.69−6.98	0.71073	0.84−1.90	0.71073
formula	$C_{14}H_{14}N_4O_6$	$C_{14}H_{14}N_4O_6$	$C_{14}H_{14}N_4O_6$	$C_{14}H_{14}N_4O_6$
M (g·mol^{-1})	334.29	334.29	334.29	334.29
T (K)	100	100	100	100
space group	$C2/c$	$C2/c$	$P\bar{1}$	$P\bar{1}$
a (Å)	11.720(5)	11.6680(5)	3.680	3.6706(4)
b (Å)	10.014(6)	9.9799(4)	7.595(6)	7.6027(8)
c (Å)	12.187(6)	12.1407(5)	12.501(9)	12.4780(12)
α (°)			85.69(5)	85.523(4)
β (°)	102.70(3)	102.747(2)	88.01(5)	88.193(4)
γ (°)			84.22(4)	84.252(5)
V (Å^3)	1395.3(12)	1378.89(10)	346.5(4)	345.31(6)
Z	4	4	1	1
ρ_{calc} (g·cm^{-3})	1.591	1.610	1.602	1.608
μ (mm^{-1})		0.129		0.128
θ range (°)		2.715−59.114		1.637−58.049
refl. measured, unique	8486, −	62005, 9393	4633, 1915	64585, 8857
R_{int}	−	0.0275	0.158	0.0252
refl. observed $I > 2\sigma(I)$	8486	7817	1365	7501
refinement method	F^2	F	F^2	F
data, parameters	8486, 178	7817, 354	1915, 172	7501, 353
GooF	1.064	1.336	1.214	0.997
R_1 observed, all data	0.0658, 0.0658	0.0159, 0.0302	0.0770, 0.1195	0.0150, 0.0274
ρ max, min	2.581, −2.088 fm·Å^{-3}	0.155, −0.146 e·Å^{-3}	1.672, −1.503 fm·Å^{-3}	0.139, −0.126 e·Å^{-3}

[a] Refinement against TOF multiwavelength data. [b] Refinement against wavelength normalized data.

difference Fourier maps ($F_{obs} - F_{calc}$) resulting in large negative residual densities in the molecular planes.

The data reduction for **1-II** was carried out according to the experimental procedure described for **1-I**, yielding a charge density data set of comparable quality. Here, 64 585 measured reflections were merged to yield a set of 8857 unique (7501 observed) reflections to a maximum sin $\theta/\lambda = 1.19$ Å^{-1}. The multipole refinement of **1-II** deviates from that described for **1-I** only in regard to the κ' parameter for the H atom involved in the SSHB, which was fixed to a standard value of 1.20 due to the fact that refinement of this parameter resulted in an unreasonable high value of approximately 2.0. All observed reflections (again there are missing reflections in the very high resolution ranges) have been used for the multipole refinement of 353 parameters to $R_1 = 0.0150$ for the observed data. The maximum and minimum residual densities are 0.139 and −0.126 e·Å^{-3} (rms = 0.027 e·Å^{-3}, all observed data, grid spacing 0.1 Å).

Theoretical Charge Density. Multipole refinements have also been performed on theoretical static structure factors calculated from the ground state wave functions up to the experimental resolutions, sin $\theta/\lambda = 1.21$ and 1.19 Å^{-1} for **1-I** and **1-II**, respectively. The ground state wave functions were obtained from single-point energy calculations on the neutron geometries using the CRYSTAL03 code,[27] full computational details being reported below. Here, the same multipole models were used as for the refinements against the experimental data, to keep the refinements as consistent as possible. The atomic coordinates, however, have been fixed to the values used for the ground state wave function calculation.

Property determinations, AIM analyses, and source function calculations have been performed using XD2006, taking as input the parameters from refinements on both the experimental and theoretical structure factors.

Computational Details. The ab initio calculations were carried out in the full periodic environment of the crystalline state using the CRYSTAL03 code.[27] Becke's three-parameter exchange functional incorporating 20% HF exchange was combined with the Perdew−Wang correlation, yielding the B3PW91 functional.[28,29] The crystalline orbitals were expanded in terms of atom-centered Gaussian type basis sets of the 6-31G** type; these include polarization functions on all atoms, namely, *p*-type functions on H and *d*-type on C, N, and O. All calculations were carried out using the crystallographic symmetry with lattice parameters fixed at the experimental values and with initial atomic positions taken from the neutron geometries. Adiabatic and diabatic potential energy profiles for one-dimensional proton motion have been calculated for the SSHBs. The adiabatic HB potentials were obtained by varying the H position along the HB vector followed by a geometry optimization for all atoms other than the H, N, and O atoms involved in the O···H···N SSHB and with O···N distances fixed to the experimental values. The diabatic HB potentials have been obtained in an analogous way from a series of single-point energy calculations on previously optimized geometries (also with O···N distances fixed to the experimental values). One-dimensional Schrödinger equations were solved for the HB potentials thereby obtained, using an in-house code. For the purpose of estimating HB energies, single-point energy calculations have been carried out also on molecular fragments isolated from the periodic structure representative of the neutron geometry using the CRYSTAL03 code with the "MOLEBSSE" instruction. For these calculations, a counterpoise correction was applied, which accounts for the change in the effective basis set due to the imposed isolation of the various molecular fragments, commonly referred to as basis set superposition error.[30] Consequently, ghost atoms have been generated in a region spanning out to 5 Å around the fragments of interest.

Results and Discussion

Neutron Diffraction. Ellipsoid plots of the neutron structures are shown in Figure 1. The structural differences between the two polymorphs have been described previously.[11] For the purposes of the current work, it suffices to

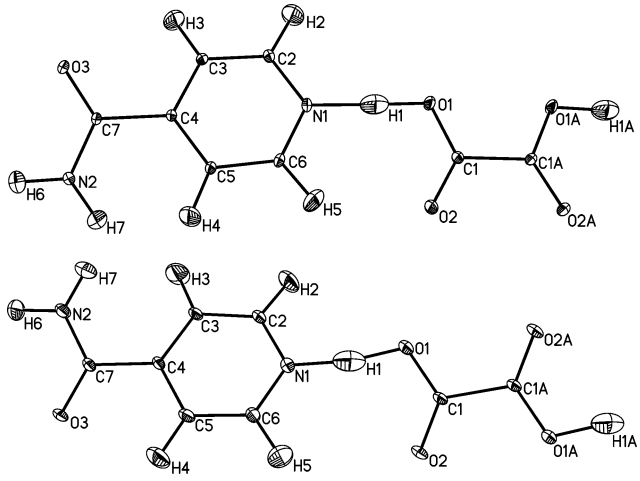

Figure 1. Asymmetric units of **1-I** (top) and **1-II** (bottom) as determined by single-crystal neutron diffraction at 100 K. For clarity, the oxalic acid molecules have been completed by applying the corresponding symmetry elements; ellipsoids at the 50% probability level.

say that both forms share the common principal features of the hydrogen bonded motif: the two oxalic acid OH groups form strong O−H···N HBs (O1−H1···N1) with two molecules of isonicotinamide, while the isonicotinamide amide groups participate in diamide HBs (N2−H6···O3) that result in the formation of (−isonicotinamide−oxalic acid−isonicotinamide−)$_n$ chains, with amide-carbonyl HBs (N2−H7···O2) cross-linking these chains into three- and two-dimensional structures in **1-I** and **1-II**, respectively (Scheme 1). In both forms, the oxalic acid moiety resides on a symmetry element, namely, a 2-fold axis in **1-I** (space group *C*2/*c*) and an inversion center in **1-II** (space group *P*1̄). The crystallographic symmetry consequently dictates a *cis*/*trans* isomerism of the oxalic acid OH groups in the two polymorphs and also renders the two SSHBs formed by each oxalic acid molecule symmetry equivalent. Another structural difference arises from the fact that the oxalic acid molecule is coplanar with the pyridine ring in **1-I**, whereas it is rotated out of the pyridine plane by approximately 28° in **1-II**.

The ADPs in both polymorphs are elongated in a direction perpendicular to the molecular plane, as expected for planar molecules in the crystalline state. In **1-II**, however, they show, for all atoms, an additional preferential orientation in the approximate direction of the **a** + **b** unit cell vector. This is likely to originate from two effects: first, from the orientation of the crystal on the diffractometer, in which the crystallographic *a*-axis was found to be approximately parallel to the vertical scan axis; and second, from an incomplete data set, which is not uncommon for a single-crystal neutron diffraction experiment, especially when the Laue symmetry is low, as is the case for **1-II**. Nevertheless, the refinement yielded reasonable positional and displacement parameters for the H atoms, which are particularly important for the analysis of the charge density in the SSHB. The neutron data indicate no disorder or delocalization of the H1 nuclear density in any of the polymorphs, the H1 atoms being found to be well localized upon examination of both the refined displacement parameters and the difference Fourier maps. The atomic displacements of H1 are slightly elongated in the general direction of the HB paths, but the overall ADPs are not significantly larger than those determined for the other H atoms in the structures and, more importantly, do not indicate any pronounced H mobility within the SSHBs (this is also true for the corresponding measurements at room temperature, in which a shortening of the O−H bonds has been observed[11,12]). Furthermore, this is consistent with the majority of exact single-crystal neutron diffraction characterizations of SSHBs in molecular compounds. To our knowledge, the only case showing a significant H mobility at low temperature was the strong intramolecular O···H···O HB in benzoylacetone.[5,31]

TABLE 2: HB Parameters Derived from Neutron Diffraction for 1 in Ångstroms and Degrees[a]

	HB	D−H	H···A	D···A	∠DHA
1-I	O1−H1···N1	1.161(3)	1.398(3)	2.5587(16)	178.2(3)
	N2−H6···O3$^{\#1}$	1.027(2)	1.894(2)	2.9165(16)	173.3(2)
	N2−H7···O2$^{\#2}$	1.013(2)	1.997(3)	3.0024(17)	171.8(2)
	C6−H5···O2	1.084(3)	2.392(3)	3.2097(18)	131.0(2)
	C5−H4···O3$^{\#3}$	1.088(3)	2.426(3)	3.278(2)	134.1(2)
	C5−H4···O2$^{\#2}$	1.088(3)	2.465(3)	3.2978(19)	132.4(2)
	C3−H3···O1$^{\#4}$	1.090(3)	2.583(3)	3.524(2)	144.0(2)
	C2−H2···O1$^{\#5}$	1.090(3)	2.609(4)	3.359(2)	125.4(2)
	C2−H2···O3$^{\#6}$	1.090(3)	2.696(4)	3.479(2)	128.4(2)
	C6−H5···O2$^{\#7}$	1.084(3)	2.674(3)	3.200(2)	109.3(2)
1-II	O1···H1···N1	1.235(5)	1.313(6)	2.539(3)	170.5(4)
	N2−H6···O3$^{\#8}$	1.036(4)	1.871(5)	2.906(3)	177.3(5)
	N2−H7···O2$^{\#9}$	1.015(3)	1.904(4)	2.903(3)	167.6(4)
	C3−H3.. .O2$^{\#9}$	1.084(5)	2.347(7)	3.290(4)	144.5(4)
	C5−H4···O3$^{\#10}$	1.085(3)	2.591(5)	3.420(3)	132.6(3)
	C3−H3···O2$^{\#11}$	1.084(5)	2.588(6)	3.256(3)	119.1(5)
	C2−H2···O1$^{\#12}$	1.092(4)	2.616(5)	3.477(3)	135.2(3)
	C2−H2···O1$^{\#13}$	1.092(4)	2.709(7)	3.216(4)	107.9(4)
	C3−H3···O1$^{\#13}$	1.084(5)	2.663(5)	3.233(3)	112.3(3)

[a] Symmetry operations. #1: $-x + 1/2, -y + 3/2, -z$; #2: $x, -y + 2, z - 1/2$; #3: $-x + 1/2, y + 1/2, -z + 1/2$; #4: $x, -y + 1, z - 1/2$; #5: $-x, -y + 1, -z + 1$; #6: $x, -y + 1, z + 1/2$; #7: $-x, -y + 2, -z + 1$; #8: $-x + 1, -y + 2, -z + 2$; #9: $x - 1, y - 1, z$; #10: $-x + 1, -y + 3, -z + 2$; #11: $x, y - 1, z$; #12: $-x + 3, -y + 3, -z + 1$; #13: $-x + 2, -y + 3, -z + 1$.

Table 2 summarizes the HB parameters obtained for the two polymorphs. The SSHB in **1-I** shows a significant elongation of the covalent O1−H1 bond to 1.161(3) Å and a short hydrogen bonding H1···N1 contact of 1.398(3) Å in a near-linear geometry. For comparison, OH groups in isolation or where involved in only weak hydrogen bonding display O−H bond lengths in the range 0.95−1.00 Å,[32] emphasizing the strong character of this SSHB. In **1-II**, this shift of H1 toward the center of the SSHB is even more pronounced, O1−H1 and H1···N1 distances of 1.235(5) and 1.313(6) Å, respectively, being found in a slightly less linear HB geometry. In view of the fact that N−H bond lengths are systematically longer than the O−H by approximately 0.05 Å,[32] this SSHB can be described as quasi-centered and will henceforward be denoted as O1···H1····N1. The moderately strong diamide HBs (H6···O3) have similar HB lengths in the two polymorphs. The amide−carbonyl interaction (H7···O2) on the other hand is shorter in **1-II** by approximately 0.1 Å. This appears to be a consequence of the aforementioned rotation of the oxalic acid molecule relative to the pyridine plane in this polymorph, accompanied by an approximately coplanar arrangement of the amide and carboxylic acid groups. In addition to the strong and moderate HBs, there are a number of weak C−H···O interactions present in **1**; Table 2 includes those for which the H···O distances are smaller than 2.8 Å. In **1-I**, the shortest C−H···O contact (H5···O2 = 2.392(3) Å) occurs between oxalic acid and a pyridine α-C−H, completing a hydrogen bonded cyclic synthon typical of pyridine−carboxylic acid adducts. This C−H···O interaction is absent in **1-II**, due to the fact that the oxalic acid molecule is rotated out of the pyridine plane in this case. Instead, an even shorter C−H···O contact (H3···O2 = 2.347(7) Å) is formed between oxalic acid and a pyridine *β*-C−H of a neighboring

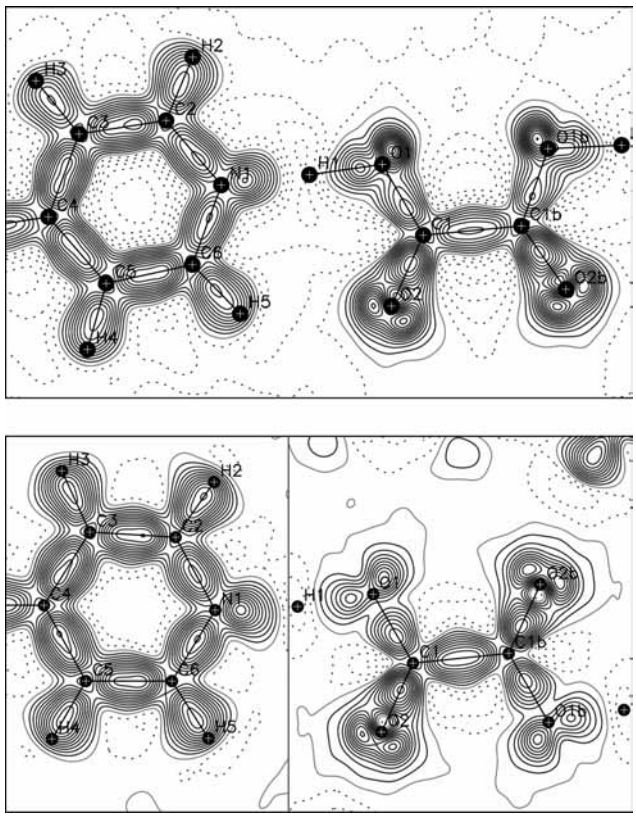

Figure 2. Dynamic model deformation density maps of **1-I** (top) and **1-II** (bottom) in the planes of the SSHBs (C1−O1−N1). A separate map has been generated for **1-II** in the plane of the pyridine ring (bottom left) as it is rotated out of the oxalic acid plane. Maps for sin $\theta/\lambda <$ 1.21 and 1.19 Å^{-1} for **1-I** and **1-II**, respectively. Positive contours - solid black; zero levels - solid gray; negative - dotted; contours at 0.05 e·Å^{-3}.

isonicotinamide molecule. Finally, as proof of the efficiency of the Laue technique at a reactor source, we note that the errors on the bond lengths and angles in **1-II** are on average only twice as large as those in **1-I** and quite acceptable, despite the crystal volume being some 50 times smaller.

Charge Density. Previous standard resolution X-ray studies have shown a strong delocalization of the electron density in the SSHBs, spanning the whole distance from O1 to N1. The discrepancy between electron density delocalization and nuclear localization was explained in terms of an overlap of the electron density originating from the H atom with charge transfer effects originating from the formation of the SSHBs.[11] The accurate determination of the total electron density distribution allows for the visualization and quantification of these charge transfer effects. Figure 2 shows the dynamic model deformation density maps ($F_{\mathrm{calc,multipole}} - F_{\mathrm{calc,spherical}}$) obtained in the planes of the SSHBs. They indeed reveal the accumulation of charge in the covalent bonds and the lone pair regions of the O and N atoms. With regard to the SSHBs, it is apparent that the addition of the H1 electron density to that originating from the O/N lone pairs and O/N···H bonds yields the electronic delocalization observed previously.

With the aim of quantifying the charge transfer on formation of the SSHBs, atomic charges have been obtained from the refined monopole, integrated Bader, and theoretical Mulliken populations. It should be noted that the charges on atoms are not uniquely defined and that absolute values can differ quite dramatically according to partitioning schemes used. Arguably, the most rigorous and unbiased method of determining an atomic

TABLE 3: Selected Net Charges[a]

	1-I			1-II		
	Monopole	Bader	Mulliken	Monopole	Bader	Mulliken
C1	+0.06	+1.36	+0.53	+0.11	+1.43	+0.54
	0.00	+1.47		−0.01	+1.47	
O1	−0.24	−1.09	−0.57	−0.18	−1.01	−0.60
	−0.23	−1.08		−0.26	−1.08	
O2	−0.44	−1.15	−0.50	−0.28	−1.08	−0.51
	−0.23	−1.12		−0.23	−1.13	
N1	−0.28	−0.99	−0.54	−0.20	−1.03	−0.53
	−0.13	−0.97		−0.18	−1.00	
H1	+0.36	+0.72	+0.46	+0.22	+0.64	+0.46
	+0.25	+0.59		+0.28	+0.58	
H6:H7	+0.17	+0.57	+0.34	+0.15	+0.47	+0.34
	+0.07	+0.47		+0.08	+0.47	
H2:H5	+0.06	+0.24	+0.17	+0.04	+0.07	+0.18
	+0.02	+0.10		+0.03	+0.10	
oxalic acid	−0.52	−0.32	−0.15	−0.26	−0.04	−0.23
	−0.41	−0.27		−0.42	−0.30	
isonicotinamide	+0.26	+0.16	+0.08	+0.13	+0.03	+0.12
	+0.20	+0.15		+0.21	+0.16	

[a] As obtained from refinements on the experimental (first row) and theoretical (second row) structure factors, Mulliken charges obtained from ground state wave function calculations assuming the neutron geometry.

charge is based upon Bader's theory of Atom in Molecules.[9] The Bader method proceeds by partitioning the molecular or crystalline space into individual atomic basins through the zero-flux surface. The integrated charges produced by this approach are often counterintuitive to "chemical sense", with atomic charges easily assuming values exceeding unity. Table 3 lists the charges for the atoms involved in the SSHB and, for comparison, the average values for the amide and pyridine H atoms. The monopole and Bader populations have been derived from the multipole refinements on the experimental and theoretical structure factors, whereas the Mulliken populations have been calculated directly from the ground state wave functions. The amount of charge transfer upon SSHB formation in the two polymorphs is best seen by comparison of the electronic populations of the various types of H atoms present in the structures. Here, a clear trend is observed toward increasing charge depletion on going from the pyridine H atoms (in isolation or involved in only weak C−H···O HBs) to the amide H atoms (involved in the moderately strong N−H···O HBs) and finally to the H atoms involved in the SSHBs. While the absolute values vary according to the method, the trends remain constant. Comparison of the charges between the two polymorphs reveals a discrepancy separating the experimentally and theoretically derived charges. While the experimental monopole and Bader charges suggest a pronounced charge transfer in **1-I** from H1 to the carboxylic acid group and the pyridine N, the theoretical charges including the Mulliken charges show only minor differences between the polymorphs. Similar results emerge for the net charge transfer from isonicotinamide to oxalic acid.

Figure 3 shows the crystal electrostatic potentials in the SSHBs as obtained from the experimental multipolar models. To increase the contrast in the maps, the potentials have been calculated after removal of the contribution due to the electropositive H1 atoms, analogous to the methodology used in the experimental charge density study of methylammonium hydrogen succinate monohydrate.[2] The resulting electrostatic potentials, the minima of which were −0.42 and −0.24 e/Å in **1-I** and **1-II**, respectively, possess magnitudes in approximate proportion with the monopole charges of the removed H atoms (Table 3). The potentials derived from the multipolar modeling of the theoretical structure factors yield notably different

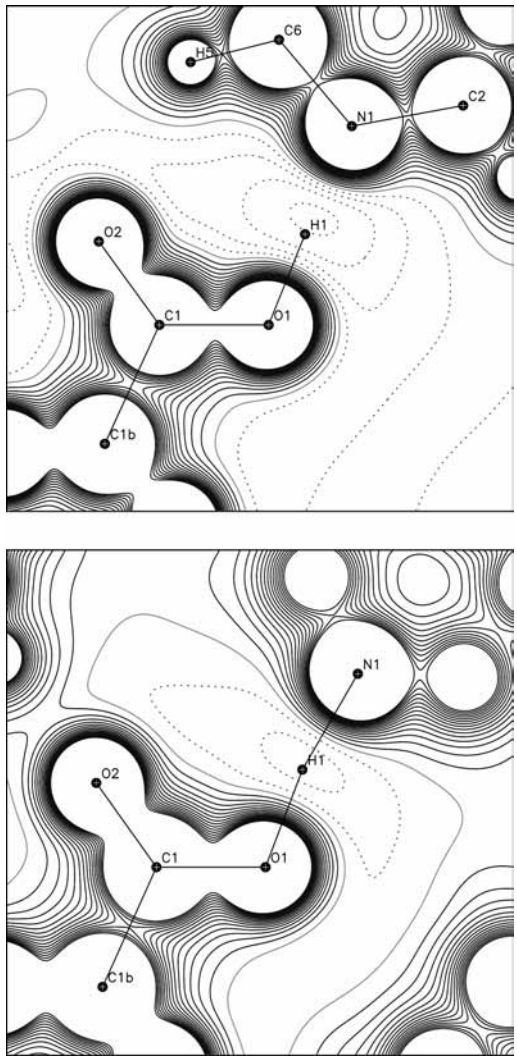

Figure 3. Electrostatic potentials calculated from the experimental charge density in the crystalline environment after removal of the contribution due to H1 in the C1−O1−N1 planes of **1-I** (top) and **1-II** (bottom): positive contours - solid black; zero levels - solid gray; negative - dotted; contours at 0.10 e·Å^{-1}.

numerical values of −0.32 and −0.35 e/Å in **1-I** and **1-II**, respectively, but the qualitative features of the maps are comparable (as shown in the Supporting Information). An interpretation of the electrostatic potential maps in the description of the SSHBs arises from the following considerations. The potential minima are located close to the geometric centers of the SSHBs in both polymorphs. This implies that in **1-I** the H1 atom, which at its equilibrium position is located closer to O1, experiences an attractive electrostatic force directed toward the potential minimum lying on the hydrogen bonding H1···N1 vector. In **1-II**, on the other hand, the H1 position roughly coincides with the potential minimum, and the hydrogen bond directed electrostatic force vanishes. In other words, in **1-I** there is a small electrostatic contribution to the actual hydrogen bonding interaction, whereas it effectively disappears in the case of the centered SSHB in **1-II**.

Topological Analysis of the Experimental Charge Density. The topological analysis of the total electron density, already employed to determine the Bader charges, allows for a characterization of the hydrogen bonding interactions in **1**. Within the AIM methodology, the criterion to distinguish a shared, covalent from a closed shell interaction is a local concentration of charge at the bond critical point (BCP) as demonstrated by a negative value for the Laplacian, $\nabla^2\rho_{BCP}$.[9] Alternatively, following from the expression $1/4\nabla^2\rho_{BCP} = V_{BCP} + 2\cdot G_{BCP}$ for the local virial theorem,[33] an interaction may be classified by the ratio $|V_{BCP}|/G_{BCP}$ of the potential to the kinetic energy density at the BCP. As the potential energy density, V, is always negative, for $|V_{BCP}|/G_{BCP} > 2$, the Laplacian of the electron density assumes a negative value, and conversely, for $|V_{BCP}|/G_{BCP} < 2$, the Laplacian becomes positive, facilitating the above classification into covalent and closed shell interactions. Espinosa et al.[34] have identified a "transit region" between covalent and "pure closed shell" interactions. The transit region is defined as $1 < |V_{BCP}|/G_{BCP} < 2$, implying that the potential energy density is in excess of the kinetic energy density ($|V_{BCP}| > G_{BCP}$) but not to the extent that it qualifies as a covalent interaction (for which $|V_{BCP}| > 2\cdot G_{BCP}$). The pure closed shell interaction is consequently defined by $|V_{BCP}|/G_{BCP} < 1$. The introduction of the concept of the transit region seems justified, in that an excess of potential over kinetic energy density at any point can be interpreted as a stabilizing criterion. Espinosa et al.[34] have also introduced the bond degree parameter, $BD = (V_{BCP} + G_{BCP})/\rho_{BCP}$, which is positive for pure closed shell interactions and negative for interactions of both shared and transit type, possessing a magnitude reflective of the strength of the respective interaction.[34]

Table 4 lists the electronic and energetic BCP properties obtained for the O···H···N SSHBs and the moderate N−H···O HBs from the multipole refinements of the experimental and theoretical structure factors, while Table 5 lists the corresponding data for the weak C−H···O HBs. Figures 4 and 5 show the plots of the experimental and theoretical negative Laplacians, $L(\mathbf{r}) = -\nabla^2\rho$, respectively, in the planes of the SSHBs. Since the energetic properties are not directly accessible from an experimental electron density distribution, they have been determined from the topological BCP properties using Abramov's approximation for G_{BCP}.[35] This has been shown to be reasonably accurate for the medium range region in which most of the BCPs are situated, corresponding to distances of approximately 0.5−2.0 Å from the nucleus. The local virial theorem has been used for determination of V_{BCP}. The covalent X−H and strong H···N interactions lie outside the medium range region, with BCP···H distances ranging from 0.25−0.40 Å, and hence the G_{BCP} and V_{BCP} values obtained are less accurate.[35]

Short, Strong HBs. The topological analysis of the experimental electron densities classifies the SSHBs in both polymorphs as shared covalent interactions from the negative values for the Laplacians at the H1···N1 BCPs. Consequently, the BCPs are located in the positive region of the negative Laplacian, $L(\mathbf{r})$, as shown in Figure 4. Moreover, the high electron densities at the BCPs emphasize the covalent character of the SSHBs. In **1-I**, the increased electron density in the H1···N1 interaction is accompanied by a reduced density in the covalent O1−H1 bond and also by a reduced charge concentration. In other words, while the H···N interaction becomes more covalent in nature, the covalence is reduced in the O−H bond. This is reflected in the plot of $L(\mathbf{r})$ shown in Figure 4 (top), where it is found that the charge concentration around H1 spans nearly the whole range between the valence shell charge concentration (VSCC) of the hydrogen-bonded heteroatoms. The term "VSCC" denotes the local maxima of charge concentration in the valence shells of atoms, effectively highlighting the lone pair and bonding regions of the density distributions, as is apparent in Figures 4 and 5. Surprisingly, the charge concentration is continuous between the H1 and N1

TABLE 4: BCP Properties of the Strong O−H···N and Moderate N−H···O Interactions[a]

	HB	R_{ij} (Å)	ρ_{BCP} (e•Å^{-3})	$\nabla^2\rho_{BCP}$ (e•Å^{-5})	λ_1 (e•Å^{-5})	λ_2 (e•Å^{-5})	λ_3 (e•Å^{-5})	G_{BCP} (Hartree•Å^{-3})	V_{BCP} (Hartree•Å^{-3})	$\lvert V_{BCP}\rvert/G_{BCP}$	BD (Hartree•e^{-1})
1-I	O1−H1	1.156	1.37	−17.2	−18.4	−18.4	19.6	0.555	−2.316	4.17	−1.29
		1.161	1.37	−12.3	−16.9	−16.8	21.4	0.787	−2.436	3.10	−1.20
	H1···N1	1.394	0.77	−3.31	−8.27	−7.97	12.9	0.365	−0.961	2.63	−0.78
		1.398	0.80	−1.94	−7.55	−7.27	12.9	0.459	−1.054	2.30	−0.75
	H6···O3	1.885	0.16	2.07	−1.09	−1.07	4.22	0.133	−0.122	0.91	0.07
		1.894	0.21	1.65	−1.26	−1.24	4.15	0.136	−0.157	1.15	−0.10
	H7···O2	1.991	0.13	1.81	−0.77	−0.76	3.34	0.111	−0.095	0.86	0.12
		1.997	0.15	1.35	−0.83	−0.81	2.99	0.097	−0.100	1.03	−0.02
1-II	O1···H1	1.233	1.08	−8.35	−12.2	−12.1	15.9	0.519	−1.622	3.13	−1.03
		1.235	1.10	−4.88	−11.7	−11.7	18.5	0.718	−1.777	2.48	−0.96
	H1···N1	1.311	0.97	−6.87	−10.3	−10.0	13.4	0.438	−1.358	3.10	−0.95
		1.313	0.97	−3.76	−9.91	−9.45	15.5	0.587	−1.438	2.45	−0.88
	H6···O3	1.867	0.21	1.61	−1.15	−1.14	3.90	0.133	−0.152	1.15	−0.10
		1.871	0.23	1.64	−1.41	−1.39	4.43	0.145	−0.175	1.21	−0.13
	H7···O2	1.902	0.19	1.51	−1.04	−1.02	3.57	0.122	−0.138	1.13	−0.08
		1.905	0.18	1.77	−1.05	−1.02	3.84	0.130	−0.136	1.05	−0.03

[a] Refinement on experimental (first row) and theoretical (second row) structure factors; λ_1, λ_2, and λ_3 are the eigenvalues obtained upon diagonalization of the Hessian matrix determining the Laplacian; bond degree parameter BD = $(V_{BCP} + G_{BCP})/\rho_{BCP}$.

TABLE 5: BCP Properties of the Weak C−H···O Interactions[a]

	HB	R_{ij} (Å)	ρ_{BCP} (e•Å^{-3})	$\nabla^2\rho_{BCP}$ (e•Å^{-5})	λ_1 (e•Å^{-5})	λ_2 (e•Å^{-5})	λ_3 (e•Å^{-5})	G_{BCP} (Hartree•Å^{-3})	V_{BCP} (Hartree•Å^{-3})	$\lvert V_{BCP}\rvert/G_{BCP}$	BD (Hartree•e^{-1})
1-I	O2···H5	2.386	0.04	1.10	−0.21	−0.17	1.47	0.055	−0.034	0.61	0.53
		2.394	0.07	0.97	−0.26	−0.20	1.43	0.054	−0.040	0.74	0.22
	O3···H4	2.420	0.05	0.91	−0.23	−0.14	1.28	0.047	−0.031	0.65	0.36
		2.428	0.06	0.87	−0.23	−0.17	1.27	0.048	−0.035	0.73	0.22
	O2···H4	2.456	0.05	0.91	−0.23	−0.14	1.28	0.048	−0.032	0.67	0.31
		2.465	0.06	0.85	−0.20	−0.14	1.19	0.046	−0.034	0.73	0.22
	O1···H3	2.596	0.03	0.45	−0.16	−0.12	0.72	0.023	−0.015	0.66	0.26
		2.588	0.04	0.55	−0.16	−0.13	0.84	0.030	−0.021	0.71	0.20
	O1···H2	2.620	0.03	0.73	−0.13	−0.06	0.91	0.036	−0.020	0.57	0.61
		2.609	0.04	0.64	−0.14	−0.08	0.87	0.034	−0.023	0.67	0.28
	O3···H2	2.688	0.02	0.58	−0.12	−0.05	0.75	0.029	−0.017	0.58	0.50
		2.699	0.03	0.51	−0.12	−0.07	0.70	0.027	−0.018	0.66	0.26
	O2···H5	2.729	0.04	0.72	−0.15	−0.10	0.97	0.037	−0.024	0.64	0.35
		2.726	0.04	0.69	−0.13	−0.08	0.90	0.036	−0.023	0.65	0.32
1-II	O2···H3	2.346	0.08	1.00	−0.30	−0.24	1.55	0.060	−0.049	0.83	0.12
		2.348	0.08	0.98	−0.30	−0.25	1.52	0.057	−0.045	0.80	0.15
	O3···H4	2.590	0.05	0.65	−0.16	−0.13	0.94	0.035	−0.025	0.72	0.21
		2.594	0.04	0.60	−0.15	−0.10	0.85	0.032	−0.022	0.68	0.24
	O2···H3	2.591	0.06	0.77	−0.17	−0.12	1.06	0.042	−0.031	0.73	0.21
		2.597	0.05	0.76	−0.16	−0.08	1.00	0.040	−0.027	0.67	0.29
	O1···H2	2.620	0.04	0.58	−0.13	−0.11	0.83	0.031	−0.022	0.71	0.21
		2.623	0.04	0.55	−0.14	−0.11	0.80	0.030	−0.021	0.70	0.22
	O1···H2	2.735	0.04	0.64	−0.12	−0.08	0.84	0.034	−0.024	0.69	0.24
		2.753	0.04	0.65	−0.12	−0.07	0.84	0.033	−0.021	0.64	0.33

[a] See Table 4 for details.

nuclei, whereas there is a small region of charge depletion in the formally covalent interaction O1−H1. Intuitively, one would expect the opposite. The charge concentration in the H1···N1 bond is partly caused by the basic N lone pair, which has a more diffuse character than the O lone pairs. The discontinuity of charge concentration in the O−H bond has been observed in other SSHBs, but is atypical for normal O−H bonds, and further indicates that this bond experiences a weakening upon formation of the SSHB.

The above findings are more pronounced in the case of the centered SSHB in **1-II**. Here, a high electron density and a negative Laplacian point to an enhanced covalence in the H1···N1 interaction, and on the other hand, a low electron density and a small negative value for the Laplacian (relative to covalent O−H bonds) point to a reduced covalence in the O1···H1 interaction. Thus, the formally covalent and hydrogen bonding interactions exhibit similar BCP properties, supporting the model of a centered HB. The plot of $L(\mathbf{r})$ in Figure 4 (bottom) shows similar features to those discussed for **1-I**, namely, charge depletion in the O1···H1 bond and a continuous region of charge concentration in the H1···N1 bond. As compared with **1-I**, the overlap region of charge concentration between H1 and N1 is increased, which is likely reflective of the shorter H1···N1 distance in this case.

Further insight into the nature of the SSHBs emerges from their energetic properties. The fact that $\lvert V_{BCP}\rvert/G_{BCP}$ is >2 for the H1···N1 interactions in both polymorphs confirms the covalent character of these SSHBs but does not really provide any further insight. However, the centered character of the SSHB in **1-II** becomes apparent from the virtually identical values for $\lvert V_{BCP}\rvert/G_{BCP}$ of 3.13 and 3.10 obtained at the O1···H1 and H1···N1 BCPs, respectively. The same conclusion can be drawn from an examination of the BD parameters, which are −1.03 and −0.95 for the O1···H1 and H1···N1 bonds, respectively.

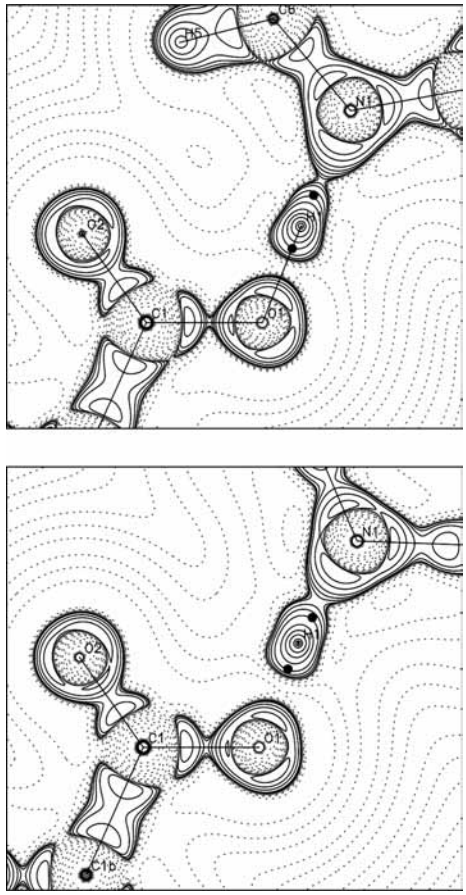

Figure 4. Plots of the experimental negative Laplacian, $L(\mathbf{r})$, in the C1−O1−N1 planes of the SSHB in **1-I** (top) and **1-II** (bottom). BCPs in the SSHB marked as black circles: positive contours - solid black; zero levels - solid gray; negative - dotted.

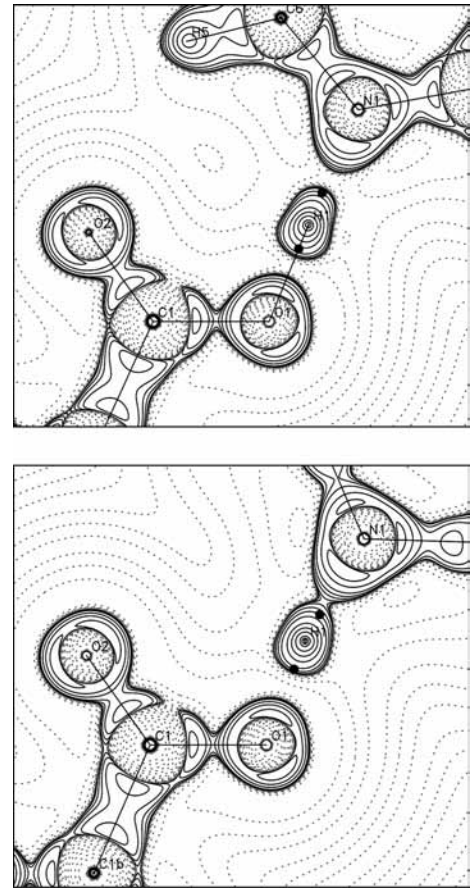

Figure 5. $L(\mathbf{r})$ from the multipole model based on refinement against the theoretical structure factors. See Figure 4 for details.

In comparison, the less centered SSHB in **1-I** leads to significantly different values of $|V_{BCP}|/G_{BCP}$ (4.17 and 2.64, respectively) and BD parameters of −1.29 and −0.78, respectively. The BD also highlights the profound difference separating the SSHBs and weaker N−H···O HBs, in that average BD parameters of −1.74 and 0 are found at the N−H and H···O BCPs, respectively.

Moderate and Weak HBs. Regarding the moderately strong N−H···O HBs, the electron densities measured at the H···O BCPs are small and tend to decrease with increasing H···O lengths (see Table 4). The Laplacian values are positive and small, as is expected for interactions of this type, and the N−H···O HBs may be classified as closed shell interactions in agreement with the classical electrostatic HB model. Values of $|V_{BCP}|/G_{BCP}$ in the H···O bonds cluster around 1, in keeping with the above-mentioned BD parameter of approximately zero. More precisely, the experimental data show $|V_{BCP}|/G_{BCP} < 1$ in **1-I** and $|V_{BCP}|/G_{BCP} > 1$ in **1-II**. The HBs are indeed shorter and hence presumably stronger in the latter polymorph, and it is noted that these values place the HBs in the pure closed shell and transit regions, respectively. However, the theoretical data discussed below show $|V_{BCP}|/G_{BCP} > 1$ for all of the N−H···O HBs. In any case, following the arguments of Espinosa et al.,[34] the N−H···O HBs all appear to fall at the borderline separating pure closed shell and transit region interactions.

The weak C−H···O HBs are included to provide a complete picture of the hydrogen bonding interactions in **1**. The electron densities found at the BCPs of such interactions are inherently low, ranging from approximately 0.08 to 0.02 e·Å^{-3} in **1**, and border the range of experimental error. The topological analyses provide bond paths for all but one of the interactions reported in Table 2, namely, the C3−H3···O1 contact in **1-II**. The BCP properties shown in Table 5 classify all C−H···O interactions as pure closed shell interactions as expected: aside from the low electron densities, the Laplacians are positive and small, ranging from 1.10 to 0.45 e·Å^{-5}, $|V_{BCP}|/G_{BCP} < 1$, so that BD > 0.

Topological Analysis of the Theoretical Charge Density. Topological analyses have also been performed on the electron densities obtained from a multipole model refinement against theoretical structure factors. The resulting BCP properties are generally in good agreement with those obtained from the experimental data. The only significant deviation in ρ_{BCP} of ∼0.05 e·Å^{-3} occurs for the H6···O3 HB in **1-I**, and all other deviations are within the error of the experimental electron density, given that the rms values of the residual density are 0.029 and 0.027 e·Å^{-3} in **1-I** and **1-II**, respectively. However, as a second derivative, the Laplacian of the electron density is more susceptible to error and reveals some differences. Most noticeably, for the SSHB in **1-I**, the VSCC between H1 and N1 is no longer continuous (Figure 5 top), while in **1-II**, the experimental features of the VSCC are reproduced (Figure 5 bottom). Furthermore, in both polymorphs, the theoretical absolute values for $\nabla^2\rho_{BCP}$ in the SSHBs are considerably smaller than their experimental counterparts. The discrepancies in the Laplacian may be due to incomplete deconvolution of the thermal motion. However, the ratio of the Laplacians obtained at the O1···H1 and H1···N1 BCPs provides very comparable values for the theoretical and experimental charge densities. Similarly, the values $|V_{BCP}|/G_{BCP}$ emerging from theory

TABLE 6: Source Contributions in % of ρ_{BCP} to the Strong O−H···N and Moderate N−H···O Interactions[a]

HB	Polymorph	H···A (Å)	ρ_{BCP} (e·Å^{-3})	*S*(H)	*S*(A)	*S*(D)	*S*(H + A)	*S*(D + H)	*S*(D + H + A)	*S*(molD)
H1···N1	**1-II**	1.311	0.97	30.8	43.6	7.9	74.4	38.7	82.3	43.4
		1.313	0.97	31.5	43.0	7.8	74.5	39.2	82.2	44.9
H1···N1	**1-I**	1.394	0.77	26.2	40.1	11.4	66.3	37.6	77.7	44.6
		1.398	0.80	27.2	39.9	11.3	67.1	38.5	78.4	45.4
H6···O3A	**1-II**	1.867	0.21	−12.6	22.2	35.1	9.6	22.5	44.7	45.1
		1.871	0.23	−5.9	26.8	30.6	20.9	24.7	51.5	43.7
H6···O3A	**1-I**	1.885	0.16	−33.4	19.8	51.0	−13.6	17.6	37.4	44.5
		1.894	0.21	−10.7	25.8	33.5	15.1	22.8	48.6	43.6
H7···O2A	**1-II**	1.902	0.19	−19.9	24.0	39.8	4.0	19.9	43.9	44.9
		1.905	0.18	−22.3	24.0	40.9	1.6	18.5	42.5	42.1
H7···O2A	**1-I**	1.991	0.13	−44.0	2.9	58.6	−41.1	14.6	17.5	45.2
		1.997	0.15	−31.3	13.1	46.2	−18.3	14.9	27.9	41.5

[a] Refinement on experimental (first row) and theoretical (second row) structure factors; HBs listed with increasing HB lengths; *S*(molD) refers to the sum of the source contributions from the donor molecule.

are smaller but result in comparable O1···H1:H1···N1 ratios. It is also noted that the theoretical BCP properties obtained here are in very good agreement with those obtained from a theoretical study on the intramolecular O···H···N SSHB in 2-(*N*-methyl-α-iminoethyl)-phenol, which exhibits O···H and H···N distances similar to **1**.[36] Finally, the BD parameters determined from theory and experiment are comparable for all interactions, save for the weak interactions exhibiting very low ρ_{BCP} values, indicating that the bond degree is a useful parameter in comparing data originating from different experiments and/or methods.

Source Function. Insight into the nature of the HBs also emerges from a different perspective, namely, by application of the source function developed by Bader and Gatti.[37] The source function describes the contribution of a local source (LS) to the electron density at any given point. The LS is defined as $LS(\mathbf{r},\mathbf{r}') = -\nabla^2\rho(\mathbf{r}')/4\pi|\mathbf{r} - \mathbf{r}'|$,[38] i.e., a distance weighted Laplacian. Meaningful information is obtained by integration of the LS over an atomic basin, leading to the source contribution (*S*) of an atom to the electron density at the reference point **r**, which is typically taken to be a BCP. An atom can act as a source ($S > 0$) or as a sink ($S < 0$) of electron density. The attraction of this method is that the source function may be obtained from experimental and theoretical charge densities without any approximation. Despite its potential use in describing bonding interactions, little application of the source function has appeared in the literature: the few studies addressing hydrogen bonding have all applied the method to theoretical charge densities.[39−42] Gatti et al. have shown that the HB classification advanced by Gilli and Gilli[43] is supported by the appearance of characteristic features in the source function, most notably by the source contribution of the H atom, *S*(H), to the density at the H···A BCP.[40] In strong and covalent HBs, *S*(H) is high and amounts to approximately 30% of ρ_{BCP}; in borderline cases between strong and moderate HBs, *S*(H) is small but positive; while in moderate electrostatic HBs, *S*(H) is negative and thus acts as a sink of electron density with respect to ρ_{BCP}. Strong HBs are further characterized by a pronounced "localization" of the source function, by which it is meant that the sum of source contributions of the atoms involved in the HB, *S*(D + H + A), is high, typically approximately 90% of ρ_{BCP} for strong covalent HBs. Moderate HBs show a more "delocalized" source function characterized by a value *S*(D + H + A) amounting to approximately 30% of ρ_{BCP}, with comparably high source contributions from atoms further away from the H···A BCP. This may be interpreted as reflecting the long-range nature of electrostatic interactions.

In the present work, the source function for the HBs present in **1** has been calculated from the experimental and theoretical charge densities. The individual source contributions to the electron density at the H···A BCPs are listed in Table 6 and visualized for the experimental values in **1-II** in Figure 6. For the O1−H1···N1 SSHB in **1-I**, the characteristic features reported by Gatti et al. for strong and covalent HBs are well reproduced, namely, a high positive source contribution of the H atom with *S*(H1) = 26.2% and also a high combined source contribution from the atoms comprising the HB with *S*(O1 + H1 + N1) = 77.7%. Both of these contributions further increase in **1-II** to values with 30.8 and 82.3%, respectively, and further support the notion that the SSHB is stronger in **1-II**. The N2−H6···O3A diamide and N2−H7···O2A amide−carbonyl HBs show features in the source function typical of moderately strong HBs of the primarily electrostatic type. Here, the source contributions of the H atoms are negative, and the combined source contributions of D, H, and A are significantly smaller than in the SSHBs. The qualitative difference between the strong and moderate HBs is also evident in Figure 6, where the SSHB (a) shows a localized source function in O1, H1, and N1, with the main contributions originating from the bonded atoms H1 and N1 as is expected of covalent bonds. The two moderate HBs (b and c), on the other hand, show more delocalized source functions with negative contributions of the H atoms. Comparison of the source functions obtained from the experimental and theoretical electron densities reveals excellent agreement for the SSHBs but considerable numerical differences for the moderately strong HBs. The errors associated with such calculations increase with the decreasing reference electron densities found at the H···O BCPs and have been discussed by Gatti and Lasi.[44]

Hydrogen Bond Potentials. The SSHB potentials were obtained from calculations that preserved the crystallographic symmetry, which means that both H atoms were moved simultaneously across the two SSHBs. As a consequence, the N···H−OOC−COO···H−N geometry was not modeled by these simulations. This approach is deemed appropriate in light of the neutron data, which show no evidence for H disorder. Due to the uncertainty as to whether adiabatic or diabatic HB potentials are a better model of the real system, both approaches have been pursued separately. The adiabatic potential assumes low H transfer frequencies to which the wider molecular geometries can adapt, while the diabatic potential conversely assumes a high frequency H transfer, to which the wider crystal structure cannot adapt. Strictly speaking, the former potentials obtained in this work are not truly adiabatic, for the intermo-

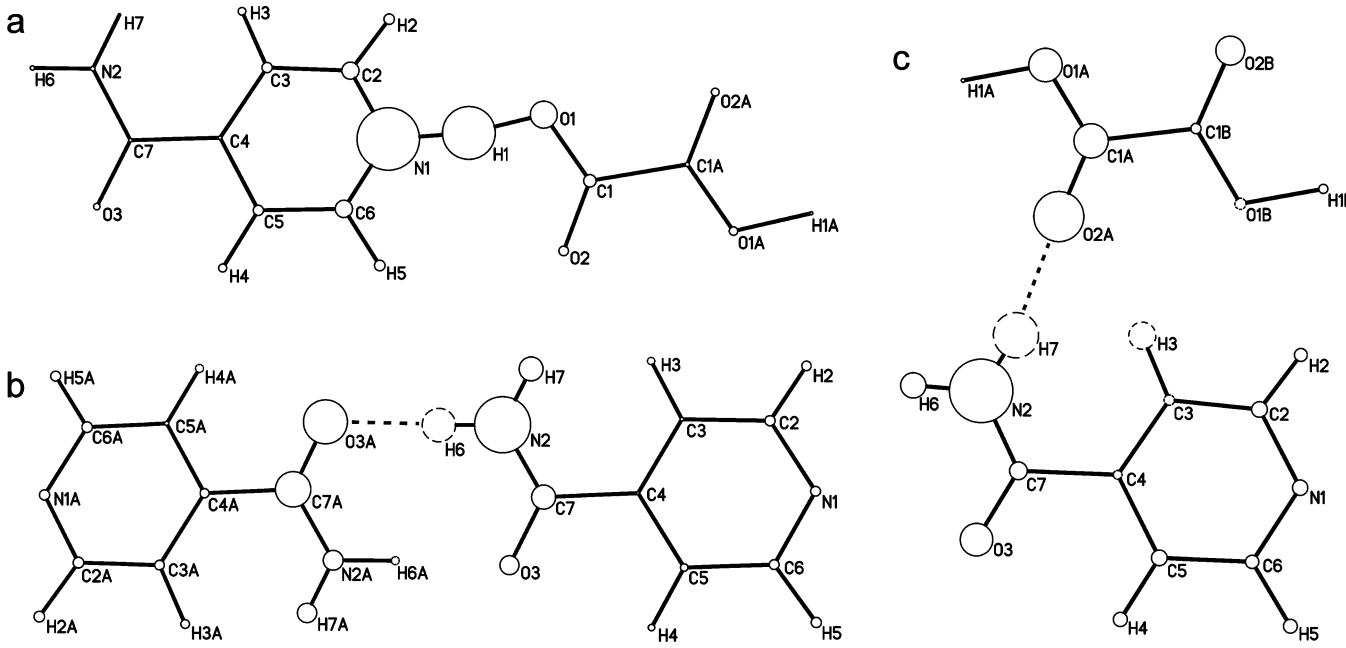

Figure 6. Experimental source contributions to the H1···N1 (a), H6···O3A (b), and H7···O2A (c) BCPs in **1-II**. The areas of the circles representing the atoms are proportional to the source contributions: positive contributions denoted by solid circles and negative by dashed circles.

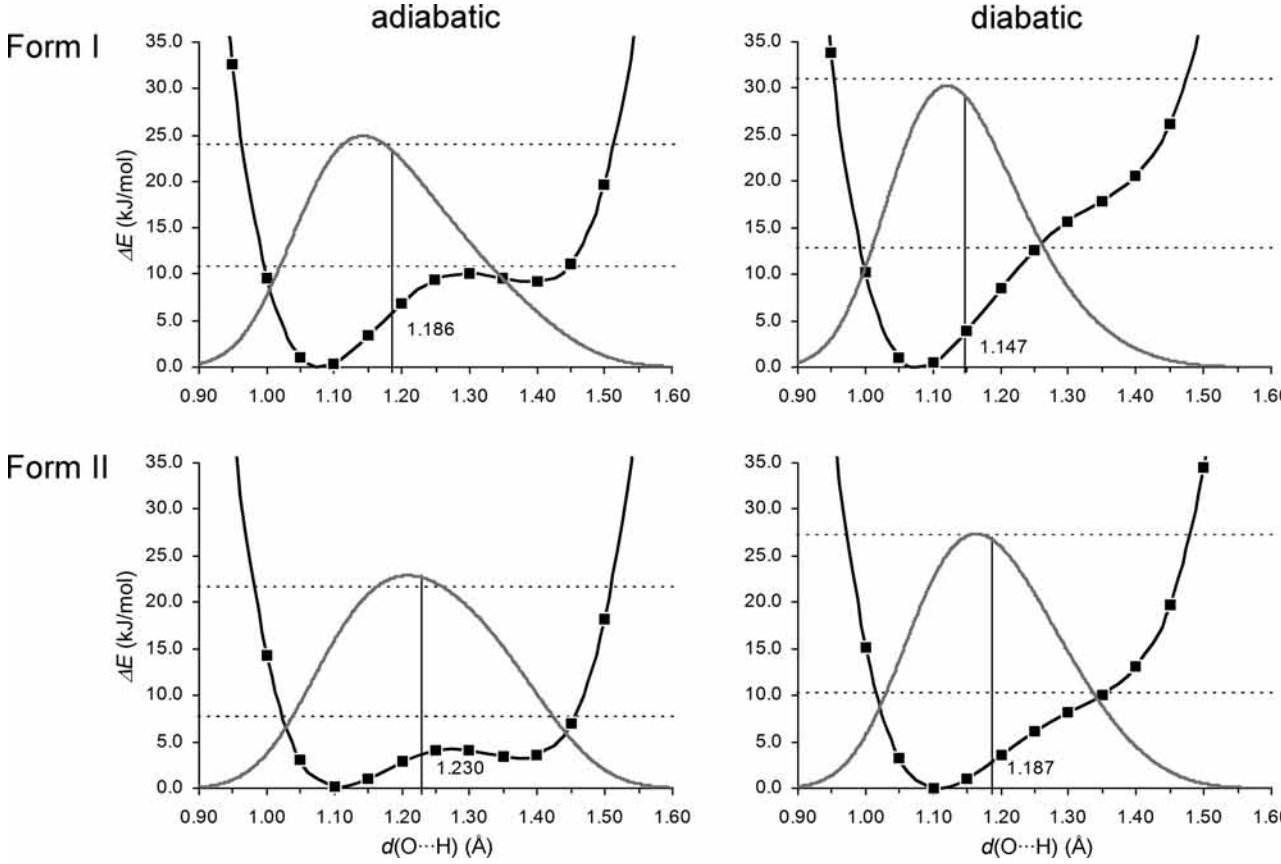

Figure 7. Adiabatic and diabatic HB potentials in **1**. Probability density distribution ($|\Psi|^2$) in gray; energy levels of the ground state and first excited state as dashed horizontal lines; and vertical lines mark the <O···H> expectation values obtained from the ground state.

lecular O···N distances were not allowed to relax. Arguably, adiabatic potentials may be more appropriate in the current compound since SSHBs are characterized by a shift toward low X−H stretching frequencies lying in the range of the internal molecular vibrations, particularly in regard to the ν(C−O) and ν(C−N) frequencies, which vary sensitively with the protonation states of the carboxylic acid and pyridine groups, respectively.

In the current case, the difference between adiabatic and diabatic HB potentials immediately becomes apparent when the potential shapes shown in Figure 7 are examined. The adiabatic potentials in both polymorphs are characterized by double well profiles, with the lower energy minimum occurring for the O−H···N configuration and a secondary local minimum occurring for the O···H−N configuration. The energy minima

are separated by barriers approximately 10 and 4 kJ/mol in height in **1-I** and **1-II**, respectively. The HB potential in **1-II** is typical of a low barrier hydrogen bond (LBHB). The diabatic potentials, meanwhile, show only one energy minimum for the O−H···N configuration; the secondary minimum is absent because the geometries of the hydrogen bonded molecules were not permitted to relax while moving the H atom away from the energetically favored configuration. As a consequence, the potentials are now typical of single-well hydrogen bonds (SWHBs). To evaluate which of the approaches is more appropriate, the properties obtained from the one-dimensional wave functions are examined. A direct approach to evaluate the HB potentials is offered by the probability density distributions, $|\Psi|^2$, and the expectation values for the H positions in the SSHBs, $\langle O\cdots H\rangle = \int |\Psi(x)|^2 x dx$, which can be compared with the structural data. In **1-I**, the experimental O−H distance lies between those found for the ground state expectation values of $\langle O\cdots H\rangle = 1.186$ and 1.147 Å in the adiabatic and diabatic potentials, respectively. In **1-II**, the experimental O−H distance agrees very well with the $\langle O\cdots H\rangle$ value of 1.230 Å in the adiabatic HB potential, while the $\langle O\cdots H\rangle$ value of 1.187 Å in the diabatic potential appears to be considerably underestimated. In this polymorph, the adiabatic approach to the calculation of the SSHB potential would therefore seem to be the more appropriate. To some extent, this is also true for **1-I**, when considering that the expectation value of 1.186 Å at 0 K found in the adiabatic potential fits the experimentally determined trend toward longer O−H distances with decreasing temperature, 1.148(4) Å at 300 K and 1.165(3) Å at 30 K.[11] Independent of the HB model, the current solid state calculations reproduce the experimentally observed elongation of the O−H bonds and the fact that this elongation is pronounced in **1-II**. Despite this good agreement with the experiment, it should be borne in mind that the HB potentials calculated here are merely models of the real system. A range of approximations and simplifications are involved, and as discussed above, the calculated potential shape ultimately depends on the computational method used and the assumptions made, such as whether to permit relaxation of the wider structure.

Hydrogen Bond Energies. HB energies may be estimated based on the approximation

$$E_{HB} \sim -0.5 V_{BCP} \quad (1)$$

proposed by Espinosa et al. for moderate and weak H···O HBs and also directly from the neutron H···O distances on the basis of the exponential fit[45]

$$E_{HB} \sim 25300 \exp(-3.6 d(H\cdots O)) \quad (2)$$

The HB energies thus obtained are listed in Table 7. Unfortunately, for the SSHBs, the Abramov approximation[35] underlying eqs 1 and 2 is not valid, and the energies are overestimated for these interactions. On the other hand, the HB energies for the moderate N−H···O HBs present in the two polymorphs can be considered as more realistic. They are approximately 20−30 kJ/mol, lying within the expected range for such interactions.[46] Furthermore, they are consistent with simple bond length considerations, in that, for **1-I**, the shorter diamide HB (N2−H6···O3) is stronger than the longer amide−carbonyl HB (N2−H7···O2), while in **1-II** the corresponding HBs have similar HB strengths, in keeping with their similar lengths in this polymorph. Comparing the HB energies obtained according to eqs 1 and 2 shows an excellent agreement, the only exception again relating to the energy of the diamide HB in **1-I**, which appears slightly underestimated when calculated from eq 1. The HB energies derived from the theoretical charge densities, given in parentheses in Table 7, increase by approximately 5 kJ/mol in the case of the diamide HBs but are in excellent agreement in the case of the amide−carbonyl HBs. Equations 1 and 2 also permit for the calculation of the C−H···O HB energies. However, due to the comparatively large error associated with estimates of such weak interactions, no individual energies are given in Table 7. It is noted only that the sums of the C−H···O energies in **1-I** and **1-II** show no significant differences, amounting in each polymorph to approximately 30 and 15 kJ/mol when determined by eqs 1 and 2, respectively. These values are substantial, being of the same scale as any individual N−H···O HB. However, within the AIM methodology the very existence of a bond path is associated with a stabilizing interaction. In contrast to that, it has been noted by Desiraju and Steiner that short C−H···O HBs, in particular, are not necessarily stabilizing interactions.[47]

TABLE 7: HB Energies for the Strong O−H···N and Moderate N−H···O Interactions in kJ/mol

	HB	H···A (Å)	E_{HB} BCP[a]	E_{HB} H···O[b]	E_{HB} calc[c]
1-I	O1−H1···N1	1.398			100
	N2−H6···O3	1.894	23.7 (30.5)	27.7	17.1
	N2−H7···O2	1.997	18.5 (19.4)	19.1	
1-II	O1···H1···N1	1.313			118
	N2−H6···O3	1.871	29.6 (34.0)	30.1	26.4
	N2−H7···O2	1.904	26.8 (26.5)	26.7	

[a] Calculated according to Espinosa et al. from the BCP properties of the experimental and theoretical (in parentheses) charge densities using eq 1.[45] [b] Calculated from neutron H···O distances using eq 2.[45] [c] Calculated by means of separate single-point energy calculations (see text).

Theoretical estimates of the HB energies have been obtained from ground state energy calculations of the periodic structures and their separate constituent molecular fragments. To model the breaking of the HB interactions, single-point energies have been calculated for the neutron-derived geometries of the periodic structure, the strongly hydrogen bonded molecular isonicotinamide−oxalic acid−isonicotinamide unit (IN−OA−IN), and the individual isonicotinamide and oxalic acid molecules. The energy differences thus obtained can be taken to correspond to the total interaction energies between the molecular units of interest, including the strong and moderate HBs, weak C−H···O interactions, and other even weaker interactions of the dispersive type. In light of their relatively small contribution to the total interaction energies, the fact that they are not necessarily stabilizing, and the fact that they are nearly impossible to quantify reliably in a molecular assembly, the C−H···O HBs are neglected to a first approximation at this point. Thus, the interaction energies are computed here only for the strong and moderate HBs present in the lattice. The energy difference separating IN−OA−IN in the crystal and the isolated IN−OA−IN unit correspond approximately to the energy required to break four N−H···O HBs, so that only a mean value for the diamide and amide−carbonyl HBs can be derived. Similarly, the energy difference separating the isolated IN−OA−IN unit and the summed energies of two isolated isonicotinamide and one isolated oxalic acid molecules corresponds to the energy of two SSHBs. The results derived from these calculations are shown in Table 7. The SSHB energies of 100 and 118 kJ/mol obtained in **1-I** and **1-II**, respectively, appear to be of a reasonable magnitude and are comparable to those in $[H_3N{-}H{-}NH_3]^+$ and $[HO{-}H{-}OH]^-$.[48] The mean N−H···O HB energies are situated at the lower end of the energy range which has been determined

from the BCP properties for these interactions. In fact, they correspond to the energies of the amide−carbonyl HBs which agree remarkably well across all methods applied. Considering the very crude estimates for the C−H···O HB energies obtained from eqs 1 and 2 would reduce the contribution of the N−H···O HBs to the interaction energies by approximately 1/3, this would also place the present N−H···O HBs in the energy regime typical of weak HBs, in contrast with the results obtained from the topological analyses.

Polymorph Formation and Stability. The ground state energies of the periodic structures can be used to estimate an energy scale for the different polymorphs. Comparison of the energies obtained from the optimized geometries and single-point energy calculations favors **1-I** over **1-II** by 4.6 and 6.6 kJ/mol, respectively. Hence, it appears that **1-I** is the energetically more stable polymorph, which would also agree with the observations from the crystallization experiments. The HB energies, on the other hand, have consistently been determined to be higher in **1-II** than in **1-I**. Also, the total interaction energies obtained from the ab initio calculations, which include the energy contributions from the weaker interactions in this compound (e.g., C−H···O, $\pi-\pi$, etc.), are higher in **1-II**. Bearing in mind that the HB and interaction energies calculated above do not necessarily correspond to the energy gain upon formation, as molecules in the crystalline state can be forced to adopt energetically disfavored geometries and close contacts, these results are not contradictory. It can only be deduced that the strengths of the intermolecular interactions may initially drive the formation of the two polymorphs, i.e., leading to the early crystallization of **1-II**, but do not ultimately determine the polymorph stability; otherwise, **1-II** should be formed exclusively. It can also be speculated that in the presence of the strong and moderate HBs the weak interactions, although contributing to the polymorph stability, are likely to have little influence on the formation of a particular polymorph. In terms of polymorph stability, it should be noted that the vibrational enthalpy and entropy are not included in the calculations. They may play an important role, but the potential significance of this omission is lessened by the fact that there is no major difference in crystal packing with respect to the type of interactions.

Conclusions

This charge density study offers strong evidence for the covalent contribution to the stabilization of the O−H···N SSHB in **1-I** and in particular to the quasicentered O···H···N SSHB in **1-II**. The evidence is considerable, arising from the topological properties of the electron densities, from the characteristics of the source functions and perhaps most convincingly from the visualization of the Laplacians, showing a continuous region of charge concentration in the H···N bonds. In **1-II**, the O1···H1 and H1···N1 BCP properties are barely distinguishable, and the SSHB can truly be described as centered. As far as we are aware, this is the first documented experimental charge density study on this type of heteronuclear SSHB, despite the fact that H transfer complexes exhibiting comparable SSHBs formed between acidic OH groups and pyridine bases have recently attracted much attention.[49−51] Also, the H atoms are well localized, and there is no evidence for significant H mobility between the hydrogen bonded molecules. This appears to be the rule rather than the exception for SSHBs in the solid state.

With respect to the interaction energies involved in the formation of the two polymorphs, the present study can offer indications only. In general, any partitioning of the total interaction energy into individual contributions is approximate and cannot quantitatively reproduce the small energy differences separating polymorphs, which are typically of the order of only a few kilojoules/mole. Importantly, this falls within the energy regime ascribed to C−H···O HBs. On the other hand, qualitative trends may indeed be obtained from such a partitioning. In the current case, the topological analyses of the experimental and theoretical charge densities and the ab initio calculations consistently indicate that the interaction energies of the strong and moderate HBs are higher in **1-II**. As discussed above, this may explain the formation of this polymorph in the first place, considering the experimental and theoretical indications that **1-I** is the energetically stable polymorph.

Acknowledgment. This work was funded through EPSRC grant TR/21615 and by the University of Glasgow. Neutron beamtime at the ISIS and ILL facilities was granted by the Science and Technology Facilities Council.

Supporting Information Available: Crystallographic information files of the neutron and high resolution X-ray structures; experimental residual electron density maps (S1); and electrostatic potentials derived from the multipolar model of the theoretical charge density (S2). This material is available free of charge via the Internet at http://pubs.acs.org.

References and Notes

(1) Pimentel, G. C.; McClellan, A. L. *The Hydrogen Bond, Chapter 8: Theory of the Hydrogen Bond*; Freeman: San Francisco, CA, 1960.
(2) Flensburg, C.; Larsen, S.; Stewart, R. F. *J. Phys. Chem.* **1995**, *99*, 10130–10141.
(3) Mallinson, P. R.; Wozniak, K.; Smith, G. T.; McCormack, K. L. *J. Am. Chem. Soc.* **1997**, *119*, 11502–11509.
(4) Madsen, D.; Flensburg, C.; Larsen, S. *J. Phys. Chem. A* **1998**, *102*, 2177–2188.
(5) Madsen, G. K. H.; Iversen, B. B.; Larsen, F. K.; Kapon, M.; Reisner, G. M.; Herbstein, F. H. *J. Am. Chem. Soc.* **1998**, *120*, 10040–10045.
(6) Rodrigues, B. L.; Tellgren, R.; Fernandes, N. G. *Acta Crystallogr.* **2001**, *B57*, 353–358.
(7) Mallinson, P. R.; Smith, G. T.; Wilson, C. C.; Grech, E.; Wozniak, K. *J. Am. Chem. Soc.* **2003**, *125*, 4259–4270.
(8) Piccoli, P. M. B.; Koetzle, T. F.; Schultz, A. J.; Zhurova, E. A.; Stare, J.; Pinkerton, A.; Eckert, J.; Hadzi, D. *J. Phys. Chem. A* **2008**, *112*, 6667–6677.
(9) Bader, R. F. W. *Atoms in Molecules - A Quantum Theory*; Oxford University Press: Oxford, U.K., 1990.
(10) Vishweshwar, P.; Nangia, A.; Lynch, V. M. *Cryst. Growth Des.* **2003**, *3*, 783–790.
(11) Schmidtmann, M.; Gutmann, M. J.; Middlemiss, D. S.; Wilson, C. C. *CrystEngComm* **2007**, *9*, 743–745.
(12) Schmidtmann, M. Ph. D. Thesis, University of Glasgow, U.K., 2008.
(13) Keen, D. A.; Gutmann, M. J.; Wilson, C. C. *J. Appl. Crystallogr.* **2006**, *39*, 714–722.
(14) Sheldrick, G. M. *Acta Crystallogr.* **2008**, *A64*, 112–122.
(15) McIntyre, G. J.; Lemée-Cailleau, M.-H.; Wilkinson, C. *Physica B* **2006**, *385−386*, 1055–1058.
(16) Campbell, J. W.; Hao, Q.; Harding, M. M.; Nguti, N. D.; Wilkinson, C. *J. Appl. Crystallogr.* **1998**, *31*, 496–502.
(17) Wilkinson, C.; Khamis, H. W.; Stansfield, R. F. D.; McIntyre, G. J. *J. Appl. Crystallogr.* **1988**, *21*, 471–478.
(18) Campbell, J.; Habash, J.; Helliwell, J. R.; Moffat, K. *Inf. Q. Protein Crystallogr.* **1986**, *18*, 23–31.
(19) Volkov, A.; Macchi, P.; Farrugia, L. J.; Gatti, C.; Mallinson, P.; Richter, T.; Koritsanszky, T. XD2006, 2006.
(20) Hansen, N. K.; Coppens, P. *Acta Crystallogr.* **1978**, *A34*, 909–921.
(21) *SAINT*; Bruker AXS Inc.: Madison, WI, 2007.
(22) Sheldrick, G. M. *SADABS*; University of Göttingen: Germany, 1997.
(23) Blessing, R. H. *Cryst. Rev.* **1987**, *1*, 3–58.
(24) Blessing, R. H. *Acta Crystallogr.* **1995**, *B51*, 816–823.
(25) Volkov, A.; Abramov, Y. A.; Coppens, P. *Acta Crystallogr.* **2001**, *A57*, 272–282.
(26) Becker, P. J.; Coppens, P. *Acta Crystallogr.* **1974**, *A30*, 129–147.

(27) Saunders, V. R.; Dovesi, R.; Roetti, C.; Orlando, R.; Zicovich-Wilson, C. M.; Harrison, N. M.; Doll, K.; Civalleri, B.; Bush, I. J.; D'Arco, Ph.; Llunell, M. *CRYSTAL03*, 2003.
(28) Becke, A. D. *J. Chem. Phys.* **1993**, *98*, 5648–5652.
(29) Perdew, J. P.; Wang, Y. *Phys. Rev. B* **1992**, *45*, 13244–13249.
(30) Boys, S. F.; Bernardi, F. *Mol. Phys.* **1970**, *19*, 553–566.
(31) Madsen, G. K. H.; McIntyre, G. J.; Schiøtt, B.; Larsen, F. K. *Chem.−Eur. J.* **2007**, *13*, 5539–5547.
(32) Steiner, T. *J. Phys. Chem. A* **1998**, *102*, 7041–7052.
(33) Bader, R. F. W.; Essen, H. *J. Chem. Phys.* **1984**, *80*, 1943–1960.
(34) Espinosa, E.; Alkorta, I.; Elguero, J.; Molins, E. *J. Chem. Phys.* **2002**, *117*, 5529–5542.
(35) Abramov, Y. A. *Acta Crystallogr.* **1997**, *A53*, 264–272.
(36) Vener, M. V.; Manaev, A. V.; Egorova, A. N.; Tsirelson, V. G. *J. Phys. Chem. A* **2007**, *111*, 1155–1162.
(37) Bader, R. F. W.; Gatti, C. *Chem. Phys. Lett.* **1998**, *287*, 233–238.
(38) Gatti, C.; Bertini, L. *Acta Crystallogr.* **2004**, *A60*, 438–449.
(39) Overgaard, J.; Schiøtt, B.; Larsen, F. K.; Iversen, B. B. *Chem.−Eur. J.* **2001**, *7*, 3756–3767.
(40) Gatti, C.; Cargnoni, F.; Bertini, L. *J. Comput. Chem.* **2003**, *24*, 422–436.
(41) Hibbs, D. E.; Overgaard, J.; Piltz, R. O. *Org. Biomol. Chem.* **2003**, *1*, 1191–1198.
(42) Sørensen, J.; Clausen, H. F.; Poulsen, R. D.; Overgaard, J.; Schiøtt, B. *J. Phys. Chem. A* **2007**, *111*, 345–351.
(43) Gilli, G.; Gilli, P. *J. Mol. Struct.* **2000**, *552*, 1–15.
(44) Gatti, C.; Lasi, D. *Faraday Discuss.* **2007**, *135*, 55–78.
(45) Espinosa, E.; Molins, E.; Lecomte, C. *Chem. Phys. Lett.* **1998**, *285*, 170–173.
(46) Deshmukh, M. M.; Gadre, S. R. *J. Phys. Chem. A* **2009**, *113*, 7927–7932.
(47) Desiraju, G. R.; Steiner, T. *The Weak Hydrogen Bond, 2.2.11 Repulsive and destabilizing C-H···O interactions*; Oxford University Press: Oxford, U.K., 1999.
(48) Steiner, T. *Angew. Chem., Int. Ed.* **2002**, *41*, 48–76.
(49) Steiner, T.; Majerz, I.; Wilson, C. C. *Angew. Chem., Int. Ed.* **2001**, *40*, 2651–2654.
(50) Cowan, J. A.; Howard, J. A. K.; McIntyre, G. J.; Lo, S. M.-F.; Williams, I. D. *Acta Crystallogr.* **2003**, *B59*, 794–801.
(51) Cowan, J. A.; Howard, J. A. K.; McIntyre, G. J.; Lo, S. M.-F.; Williams, I. D. *Acta Crystallogr.* **2005**, *B61*, 724–730.

JP9067813